

# Organometallic Wires Constructed from Transitional Metals and Anthracene: A Theoretical Study

Xianlong Wang, Xiaohong Zheng and Zhi Zeng\*

*Key Laboratory of Materials Physics, Institute of Solid State Physics,  
Chinese Academy of Sciences, Hefei 230031, P.R. China*

(Dated: February 23, 2024)

## Abstract

The properties of organometallic wires  $[\text{TM}_2(\text{Ant})]_\infty$  constructed with transitional metals (TM = Sc, Ti, V, Cr, Mn and Fe) and anthracene (Ant) are investigated by first-principles calculations. As the gap between HOMO (Highest Occupied Molecular Orbital) and LUMO (Lowest Unoccupied Molecular Orbital) of Ant is much smaller than that of benzene (Bz), much larger charge transfer (CT) occurs between TMs and Ant, which results in much more diverse magnetic properties in  $[\text{TM}_2(\text{Ant})]_\infty$  than in  $[\text{TM}(\text{Bz})]_\infty$ . Particularly,  $[\text{V}_2(\text{Ant})]_\infty$  and  $[\text{Cr}_2(\text{Ant})]_\infty$  are found to be half-metallic ferromagnets. As a result of this and the better structural stability, compared with  $[\text{TM}(\text{Bz})]_\infty$ ,  $[\text{TM}_2(\text{Ant})]_\infty$  (like  $[\text{V}_2(\text{Ant})]_\infty$  and  $[\text{Cr}_2(\text{Ant})]_\infty$ ) may be better candidates of spintronic devices. Furthermore, as the HOMO-LUMO gap of small pieces of graphene (SPG), such as pentacene and coronene, decreases with the increase of polycyclic number, the CT effects may also fit for the TM-SPG sandwich polymers which can also act as good spintronic materials.

---

\* Correspondence author: zzeng@theory.issp.ac.cn

## I. INTRODUCTION

One-dimensional organometallic sandwich polymers (OSPs) have attracted wide interests in recent years due to their potential applications in spintronic devices and information storage [1–16]. One of the extensively studied systems is  $\text{TM}_n\text{Bz}_{n+1}$  which demonstrates versatile properties. The property diversity arises from two facts. On one hand, the properties of  $[\text{TM}(\text{Bz})]_\infty$  are highly dependent on the TM ions. For example,  $[\text{V}(\text{Bz})]_\infty$  and  $[\text{Mn}(\text{Bz})]_\infty$  are ferromagnetic half-metals, while  $[\text{Cr}(\text{Bz})]_\infty$  is a nonmagnetic insulator. On the other hand, the type of organic molecules can also significantly influence the properties of the one-dimensional OSPs. For example, no magnetic moment appears in  $[\text{Mn}(\text{Cp})]_\infty$  (Cp = cyclopentadienyl), while  $[\text{Cr}(\text{Cp})]_\infty$  has a ferromagnetic ground state.[10–12] It is believed that the ferromagnetism observed in such OSPs (like  $\text{V}_n\text{Bz}_{n+1}$ [1]) may qualify them as good materials for spin polarized transport.[4–7]

Because of the abundant magnetic properties and the possibility as candidates for spintronic devices and information storage, recently, the study on the one-dimensional OSPs has been extended to the cases of TM-pentalene (Pn), TM-naphthalene (Np) and TM-Ant.[13–16] The sandwich like clusters of TM-Np and TM-Ant were firstly synthesized in 1999.[13] Further theoretical investigations showed that  $[\text{V}_2(\text{Ant})]_\infty$  is a half-metallic ferromagnet. Since in  $[\text{TM}_2(\text{Ant})]_\infty$ , the Ant are connected by two TM ions, as shown in Fig 1(a), compared with  $[\text{TM}(\text{Bz})]_\infty$  and  $[\text{TM}(\text{Cp})]_\infty$ , it should have better stability and conductivity and it may be more suitable for spintronic devices and information storage. Note that, previous theoretical investigation pointed out a possible structural transition from  $D_{6h}$  to  $D_2$  symmetry appearing on  $\text{V}_n\text{Bz}_{n+1}$ . [4] Consequently, systematic investigation on this kind of polymers is quite interesting and necessary. Therefore, in this work, the structural, electronic and magnetic properties of  $[\text{TM}_2(\text{Ant})]_\infty$  (TM=Sc, Ti, V, Cr and Mn) are investigated by first principles calculations. We find that magnetic properties in  $[\text{TM}_2(\text{Ant})]_\infty$  are much different from those in  $\text{TM}(\text{Bz})_\infty$  and the difference arises from the different HOMO-LUMO gap of the organic molecules and the subsequent different CT between the TMs and the organic molecules. Especially, we find that  $[\text{V}_2(\text{Ant})]_\infty$  and  $[\text{Cr}_2(\text{Ant})]_\infty$  are half metals with the 100% spin polarized density of states (DOS) around the Fermi level, which is of great importance for spin transport.

## II. COMPUTATIONAL DETAILS

Full-electron density functional theory (DFT) implemented in the Dmol<sup>3</sup> package [17, 18] is used in our calculations. The Perdew, Burke, and Ernzerhof (PBE) [19] functional is used for exchange and correlation interaction in the generalized gradient approximation (GGA). The basis set is composed of double numerical basis and a polarized function (DNP) is chosen. The supercell is chosen as  $20 \times 20 \times c$  Å<sup>3</sup>, where  $c$  is the lattice constant along the periodic direction and is varied for different TM cases [see Table I]. The corresponding Brillouin zone is sampled by a  $1 \times 1 \times 50$  Monkhorst and Pack grid.[20] All structures are fully relaxed.

In order to investigate the different magnetic configurations and Peierls transition in  $[\text{TM}_2(\text{Ant})]_\infty$ , a supercell containing four TMs and two Ants are used. For each kind of  $[\text{TM}_2(\text{Ant})]_\infty$ , as shown in Figs. 1(b)-(f), five magnetic configurations are considered. The combination of two characters  $XY$  ( $X$  and  $Y$  correspond to  $N$ (non-magnetic),  $F$ (ferromagnetic) and  $A$ (anti-ferromagnetic)) are adopted for representing the related magnetic configurations, with  $X$  and  $Y$  describing the intralayer and interlayer magnetic coupling of TM atoms, respectively. For example, as shown in Fig. 1(d),  $FA$  means the ferromagnetic coupling between the inner layer TM atoms and the anti-ferromagnetic coupling between two nearest neighbor layers.

## III. RESULTS AND DISCUSSIONS

After full relaxation, the calculated structural, electronic and magnetic properties of  $[\text{TM}_2(\text{Ant})]_\infty$  are summarized in Table I. Peierls transition does not occur in  $[\text{TM}_2(\text{Ant})]_\infty$ , and no magnetic moment is observed in the cases of  $[\text{Sc}_2(\text{Ant})]_\infty$  and  $[\text{Mn}_2(\text{Ant})]_\infty$ . In contrast, Ti and Fe are spin polarized, but the magnetic ground states of  $[\text{Ti}_2(\text{Ant})]_\infty$  and  $[\text{Fe}_2(\text{Ant})]_\infty$  are  $FA$  and  $AF$ , respectively. Hence, the total magnetic moments of  $[\text{Ti}_2(\text{Ant})]_\infty$  and  $[\text{Fe}_2(\text{Ant})]_\infty$  supercells are zero. In addition, our calculations predict that  $FF$  is the ground state of both  $[\text{V}_2(\text{Ant})]_\infty$  and  $[\text{Cr}_2(\text{Ant})]_\infty$ , and that the supercells of  $[\text{V}_2(\text{Ant})]_\infty$  and  $[\text{Cr}_2(\text{Ant})]_\infty$  respectively possess a magnetic moment of  $2.00\mu_B$  and  $0.96\mu_B$  per TM ion, with a finite negative magnetic moment formed on the Ant part. Further analysis shows that  $[\text{V}_2(\text{Ant})]_\infty$  and  $[\text{Cr}_2(\text{Ant})]_\infty$  are half-metallic ferromagnets which can be seen from

the band structures of  $[\text{V}_2(\text{Ant})]_\infty$  and  $[\text{Cr}_2(\text{Ant})]_\infty$  shown in Figs. 2(a) and 2(b). The  $[\text{V}_2(\text{Ant})]_\infty$  total DOS and the partial DOS of V  $3d$  are shown in Fig. 2(c). It is found that the 100% spin-polarized DOS around Fermi level mainly come from the V  $3d$  orbitals, with small contribution from the C  $2d$ . A gap of 0.76 eV and 1.25 eV for  $[\text{V}_2(\text{Ant})]_\infty$  and  $[\text{Cr}_2(\text{Ant})]_\infty$  respectively is observed in the spin majority channel. Thus,  $[\text{V}_2(\text{Ant})]_\infty$  and  $[\text{Cr}_2(\text{Ant})]_\infty$  may be good candidates for spintronic devices and information storage. Note that our results on  $[\text{V}_2(\text{Ant})]_\infty$  presented here agree well with former calculations.[16]

In both  $[\text{TM}_2(\text{Ant})]_\infty$  and  $[\text{TM}(\text{Bz})]_\infty$ , TMs are located in a crystal field with  $D_{6h}$  symmetry. Under  $D_{6h}$  symmetry crystal field, as shown in Fig. 3(a), TMs  $d$  orbital splits into a  $a_1$  ( $d_{3z^2-r^2}$ ), 2-fold  $e_2$  ( $d_{xy}$  and  $d_{x^2-y^2}$ ) and  $e_1$  ( $d_{xz}$  and  $d_{yz}$ ) orbitals. In the meantime, both Ant and Bz containing 14 and 6 C atoms obey the Hückel rule, which means that a stable aromatic molecule should have  $4m+2$  carbon atoms (where  $m$  is an integer). However, the magnetic behaviors of  $[\text{TM}_2(\text{Ant})]_\infty$  are totally different from those of  $[\text{TM}(\text{Bz})]_\infty$ . [7] For example,  $[\text{Mn}(\text{Bz})]_\infty$  is a ferromagnet with  $1.0\mu_B$  magnetic moment per Mn ions, and non-magnetic state is the ground state of  $[\text{Cr}(\text{Bz})]_\infty$ . Whereas, this situation is reversed in  $[\text{TM}_2(\text{Ant})]_\infty$ , since  $[\text{Mn}_2(\text{Ant})]_\infty$  do not show any magnetic moment while Cr ions of  $[\text{Cr}_2(\text{Ant})]_\infty$  are ferromagnetically spin-polarized with  $1\mu_B$  magnetic moment. Both  $[\text{V}(\text{Bz})]_\infty$  and  $[\text{V}_2(\text{Ant})]_\infty$  are a spin-polarized sandwich polymers, but the magnetic moments of V ions in  $[\text{V}(\text{Bz})]_\infty$  and  $[\text{V}_2(\text{Ant})]_\infty$  are approximately  $1.0\mu_B$ [7] and  $2.0\mu_B$ , respectively. An interesting question arises from these results: Why is there so big difference in the magnetic properties of  $[\text{TM}_2(\text{Ant})]_\infty$  and  $[\text{TM}(\text{Bz})]_\infty$ ?

Further analysis shows that, compared with  $[\text{TM}(\text{Bz})]_\infty$ , there is a larger CT between TMs and Ant. We find that the magnetic properties of  $[\text{TM}_2(\text{Ant})]_\infty$  are attributed to the CT effect which was once proved to be responsible for the magnetic behaviors of  $[\text{TM}(\text{Cp})]_\infty$ . [12] For example, in  $[\text{V}(\text{Bz})]_\infty$ , V ( $3d^34s^2$ ) has five valence electrons occupy the  $d$  orbitals with two and three electrons respectively occupying the  $a_1$  and doubly degenerate  $e_2$  orbitals, because of two  $s$  electrons fill  $3d$  shell[5]. Hence, one unpaired electron exists in  $e_2$  orbitals, and  $[\text{V}(\text{Bz})]_\infty$  shows a magnetic moment of  $1.0\mu_B$  on each V ion. However, in  $[\text{V}_2(\text{Ant})]_\infty$ , one electron at V  $d$  orbital is transferred to Ant, and  $e_2$  has two unpaired electrons. Thus, V ions in  $[\text{V}_2(\text{Ant})]_\infty$  possess a  $2.0\mu_B$  magnetic moment. In order to illustrate this effect more clearly, calculations are performed, with the unit cell containing two TMs and one Ant and the initial magnetic coupling of two TMs arranged as ferromagnetic. For each  $[\text{TM}_2(\text{Ant})]_\infty$ ,

the calculated total unit-cell magnetic moments per TM are shown in Fig. 3(b), in which the magnetic moments and schematic occupation of valence electrons obtained by CT model are also presented. We can find that our calculated results agree well with the CT model. Furthermore,  $[\text{TM}_2(\text{Ant})]_\infty$  and  $[\text{TM}(\text{Cp})]_\infty$  are quite similar in magnetic properties, since Cp containing 5 C atoms does not obey the Hückel rule, Cp tends to get one additional electron from TMs. Therefore, CT occurs in  $[\text{TM}(\text{Cp})]_\infty$ . [12] However, according to Hückel rule, Ant is a stable aromatic molecule. We want to inspect why there is so big CT in  $[\text{TM}_2(\text{Ant})]_\infty$ . Generally, the key factors determining the CT in this kind of polymers are: (1) the average number of carbon atom (ANC) per TM; (2) the strength of frontier orbital hybridization. From  $[\text{TM}(\text{Bz})]_\infty$  to  $[\text{TM}_2(\text{Ant})]_\infty$ , the ANC increases from six to seven. This small change of ANC should not induce large CT difference between  $[\text{TM}(\text{Bz})]_\infty$  and  $[\text{TM}_2(\text{Ant})]_\infty$ . Then the large CT in  $[\text{TM}_2(\text{Ant})]_\infty$  might arise from the second factor.

Our calculations show that the HOMO-LUMO gap of Ant is 2.7 eV, which is smaller than that of Bz(5.5 eV). Comparing with Bz, the LUMO of Ant is much closer to the HOMO of TM ions. Thus, the frontier orbital hybridization between TMs and Ant is much stronger in  $[\text{TM}_2(\text{Ant})]_\infty$  than in  $[\text{TM}(\text{Bz})]_\infty$  and the CT appears on  $[\text{TM}_2(\text{Ant})]_\infty$ . This is also illustrated clearly in Figs. 3(c) and 3(d), where the partial DOS of TM 3d and Ant C 2p are shown. Taking Fermi level as the reference, the HOMO of both Bz and Ant are localized around -5.5 eV. However, as the gap of Ant is smaller than that of Bz, the minimum energy of hybridization of V 3d and C 2p electrons in  $[\text{V}_2(\text{Ant})]_\infty$  is -4 eV, which is lower than that of  $[\text{V}(\text{Bz})]_\infty$  (-3 eV). Thus, as shown in Fig 3(c) and (d), compared with  $[\text{V}(\text{Bz})]_\infty$ , the minority electrons of V in  $[\text{V}_2(\text{Ant})]_\infty$  is transferred to Ant, which can also be found in  $[\text{V}(\text{Cp})]_\infty$ . [12] Consequently, from  $[\text{V}(\text{Bz})]_\infty$  to  $[\text{V}_2(\text{Ant})]_\infty$ , the magnetic moment of V ion increases from  $1\mu_B$  to  $2\mu_B$ . The schematic view of this opinion is also shown in Fig. 3, where the frontier orbitals (HOMO and LUMO) of Bz, V and Ant are approximately shown in the left, middle and right, respectively. The bigger arrow means the larger CT in  $[\text{TM}(\text{Bz})]_\infty$  than that in  $[\text{TM}(\text{Bz})]_\infty$ .

Double exchange (DE) was attributed as one of the ferromagnetic origins of the in  $[\text{TM}(\text{Bz})]_\infty$  and  $[\text{TM}_2(\text{Pn})]_\infty$ . [7, 15] However, in  $[\text{V}(\text{Bz})]_\infty$ , the ferromagnetic state was believed to arise from the negative polarization of carbon atoms since magnetic moments anti-polarized by TMs appears on benzene. [8] In addition, in  $[\text{V}(\text{Cp})]_\infty$ , the ferromagnetism originates from the CT effects since there is CT between TMs and Cp. [12] In the cases of

$[V_2(\text{Ant})]_\infty$  and  $[\text{Cr}_2(\text{Ant})]_\infty$  that are studied in this work, strong coupling between TMs and Ant within the energy range of -4 to 0 eV can be found [see Figs. 2(c) and 3(d)]. Furthermore, the wave functions at the  $\Gamma$  point of  $[V_2(\text{Ant})]_\infty$  and  $[\text{Cr}_2(\text{Ant})]_\infty$  near the Fermi level also confirm the strong TMs-Ant coupling. Therefore, by comparing CT and negative polarization effect, it can conclude that the DE may be mainly responsible for the ferromagnetism.

Furthermore, Ant can be considered as a small piece of graphene (SPG) with multi-Bzs. SPG with more benzene rings, such as coronene and pentacene (Pe), can also be used for constructing this kind of sandwich like nanostructures and nanowires. As a matter of fact, the sandwich like TM-corroene polymers have already been synthesized.[21, 22] Such kind of polymers built with SPG and TMs may also be suitable materials for spintronic devices and information recording. Except for the properties of better stability and conductivity mentioned at the beginning, as shown in Figs. 4(a) and 4(b), TM-SPG polymers can be built into warped and branched structures. In Fig. 4(a), the relaxed structure of  $\text{Sc}_4\text{V}_4(\text{Ant})_5$  cluster are shown. As the radius of Sc is larger than the that of V,  $\text{Sc}_4\text{V}_4(\text{Ant})_5$  cluster shows a warp structure. By co-doping and introducing TM defects, warped structure can be realized in this kind of sandwich polymers. Fig. 4(b) shows the schematic branched structure constructed with Pe, Bz and TMs. In fact, warped and branched structures already achieved in carbon nanotubes and nanowires[23, 24] are central to the design of nanodevices and nanocircuits. While the different shapes and versatile properties exhibited by the sandwich like TM-SPG nanostructures and nanowires may qualify them as promising building blocks for spintronics devices and information storage. As the HOMO-LUMO gap of SPG decrease with the size increase of SPG, the CT effects and magnetic behaviors in the  $[V_2(\text{Ant})]_\infty$  may also exists in TM-SPG. Thus, further experimental and theoretical investigations are highly suggested in this interesting field.

#### IV. CONCLUSION

In conclusion, the properties of  $[\text{TM}_2(\text{Ant})]_\infty$  are investigated by first principles calculations. As the HOMO-LUMO gap of Ant is smaller than that of Bz, there is a large CT in  $[\text{TM}_2(\text{Ant})]_\infty$ , which results in different magnetic behaviors in  $[\text{TM}_2(\text{Ant})]_\infty$  from  $\text{TM}(\text{Bz})_\infty$ . Especially,  $[V_2(\text{Ant})]_\infty$  and  $[\text{Cr}_2(\text{Ant})]_\infty$  exhibit 100% spin polarized DOS around Fermi level

which is of great importance for spin transport. Furthermore, we indicate that CT effect and magnetic behaviors shown in  $[V_2(\text{Ant})]_\infty$  may also exist in TM-SPG. Finally, due to the excellent stability, conductivity and unique shape (like branch and warp) that can be possibly realized, TM-SPG may be prospective materials for spintronics and information storage.

## ACKNOWLEDGEMENTS

This work was supported by the National Science Foundation of China under Grant No 10774148, No 10904148 and No 10847162, the special Funds for Major State Basic Research Project of China(973), Knowledge Innovation Program of Chinese Academy of Sciences, and Director Grants of CASHIPS. Part of the calculations were performed in Center for Computational Science of CASHIPS and the Shanghai Supercomputer Center.

- 
- [1] K. Miyajima, A. Nakajima, S. Yabushita, M.B. Knickelbein and K. kaya, J. AM. Chem. Soc. **126**, 13202 (2004)
  - [2] J.T. Lyon and L. Andrews, J. Phys. Chem. A **109**, 431 (2005)
  - [3] K. Miyajima, S. Yabushita, M.B. Knickelbein and A. Nakajima, J. AM. Chem. Soc. **129**, 8473 (2007)
  - [4] J.L. Wang, P.H. Acioli and J. Jellinek, J. AM. Chem. Soc. **127**, 2812 (2005)
  - [5] V.V. Maslyuk, A. Bagrets, V. Meded, A. Arnold, F. Ever, M. Brandbyge, T. Bredow and I. Mertig, Phys. Rev. Lett.**97**, 097201 (2006).
  - [6] M. Kolehmainen, M. Paulsson and M. Brandbyge, Phys. Rev. Lett.**98**, 197202 (2007).
  - [7] H.J. Xiang, J.L. Yang, J.G. Hou and Q.S. Zhu, J. AM. Chem. Soc. **128**, 2310 (2006)
  - [8] H.M. Weng, T. Ozake and K. Terakura, J. Phys. Society of Japan **77**, 014301 (2008)
  - [9] H. Weng, T. Ozaki and K. Terakura, Phys. Rev.B **79**, 235118 (2009).
  - [10] S. Nagao, A. Kata and A. Nakajima, J. AM. Chem. Soc. **122**, 4221 (2000)
  - [11] L.P. Zhou, S.W. Yang, M.F. Ng, M.B. Sullivan, V.B.C. Tan and L. Shen, J. AM. Chem. Soc. **130**, 4023 (2008)

- [12] L. Shen, S.W. Yang, M.F. Ng, V. Ligatchev, L.P. Zhou and Y.P. Feng, J. AM. Chem. Soc. **130**, 13956 (2008)
- [13] T. Kurikawa, H. Tkeda, M. Hirano, K. Judai, T. Arita, S. Nagao, A. Nakajima and K. Kaya, Organometallics. **18**, 1430 (1999)
- [14] T.J. Katz and N.J. Acton, J. AM. Chem. Soc. **94**, 3281 (1972)
- [15] X.J. Wu and X.C. Zeng, J. AM. Chem. Soc. **131**, 14246 (2009)
- [16] L. Wang, Z.X. Cai, J.Y. Wang, J. Lu, G.F. Luo, L. Lai, J. Zhou, R. Qin, Z.X. Gao, D.P. Yu, G.P. Li, W.N. Mei, and S. Sanvito, Nano Letters **8**, 3640 (2008)
- [17] B. Delly, J. Chem. Phys. **92**, 508 (1990)
- [18] B. Delly, J. Chem. Phys. **113**, 7756 (2000)
- [19] J.P. Perdew, K. Burke, and M. Ernzerhof, Phys. Rev. Lett. **77**, 3865 (1996).
- [20] H.J. Monkhorst and J.D. Pack, Phys. Rev. B **13**, 5188 (1976).
- [21] B.P. Pozniak and R.C. Dunbar, J. AM. Chem. Soc. **119**, 10439 (1997)
- [22] N.R. Foster, G.A. Gieves, J.W. Buchanan, N.D. Flynn and M.A. Duncan, J. Phys. Chem. A **104**. 11055 (2000)
- [23] J. Li, C. Papadopoulos and J. Xu, nature **402**. 253 (1999)
- [24] G.W. Meng, Y.J. Jung, A. Cao, R. Vajtai and P.M. Ajayan, Proc. Natl. Acad. Sci. USA **102**. 7074 (2005)

TABLE I: The lattice constant in the  $c$  axial direction, the electronic ground state (BS), the band gap for semiconductor and half metal cases, the total supercell magnetic moment (M) per TM and valence electron distribution (VED) of  $[\text{TM}_2(\text{Ant})]_\infty$  (TM= Sc, Ti, V, Cr, Mn and Fe).

meV	$c(\text{\AA})$	GS	band gap (eV)	$M(\mu_B)$	VED
Sc	7.89	$NN(\text{metal})$	0.00	0.00	$3d^14s^2$
Ti	7.37	$FA(\text{metal})$	0.00	0.00	$3d^24s^2$
V	7.01	$FF(\text{half metal})$	0.76(direct)	2.00	$3d^34s^2$
Cr	6.79	$FF(\text{half metal})$	1.25(direct)	0.96	$3d^44s^2$
Mn	6.64	$NN(\text{semicond})$	0.66(direct)	0.00	$3d^54s^2$
Fe	6.87	$AF(\text{metal})$	0.00	0.00	$3d^64s^2$

FIG. 1: The top view of  $[\text{TM}_2(\text{Ant})]_\infty$  (a) and five initial magnetic structures used in our calculations: (b)  $NN$ , (c)  $FF$ , (d)  $FA$ , (E)  $AF$ , (f)  $AA$ . Blue circles and arrows respectively represent the non-magnetic state and magnetic moment direction of TMs. Arrows marked by X and Y denote the magnetic interactions inside one layer and between nearest two layers, respectively.

FIG. 2: Spin-resolved electronic band structures for (a)  $[\text{V}_2(\text{Ant})]_\infty$  and (b)  $[\text{Cr}_2(\text{Ant})]_\infty$ , respectively. (c) the total DOS and V  $3d$  partial DOS of  $[\text{V}_2(\text{Ant})]_\infty$ .

FIG. 3: (a) the splitting of TMs  $d$  orbitals under the  $D_{6h}$  symmetry crystal field. (b) the calculated magnetic moments (per TM ions) of ferromagnetic  $[\text{TM}_2(\text{Ant})]_\infty$  unit cell. The TMs electrons configurations and magnetic moments predicted by CT-module are also shown in (b). (c) the total V  $3d$  and C  $2p$  partial DOS of  $[\text{V}(\text{Bz})]_\infty$ . (d) the total V  $3d$  and C  $2p$  partial DOS of  $[\text{V}_2(\text{Ant})]_\infty$ . Schematic HOMO and LUMO positions of Bz, V and Ant are shown in the left, middle and right, respectively. The wider blue arrow means a larger CT between V and Ant.

FIG. 4: (a) Side view of the relaxed  $\text{Sc}_4\text{V}_4\text{Ant}_5$  cluster. (b) The schematic structure of branched sandwich clusters constructed by pentacene, benzene and TMs.

Fig. 1 Wang.eps

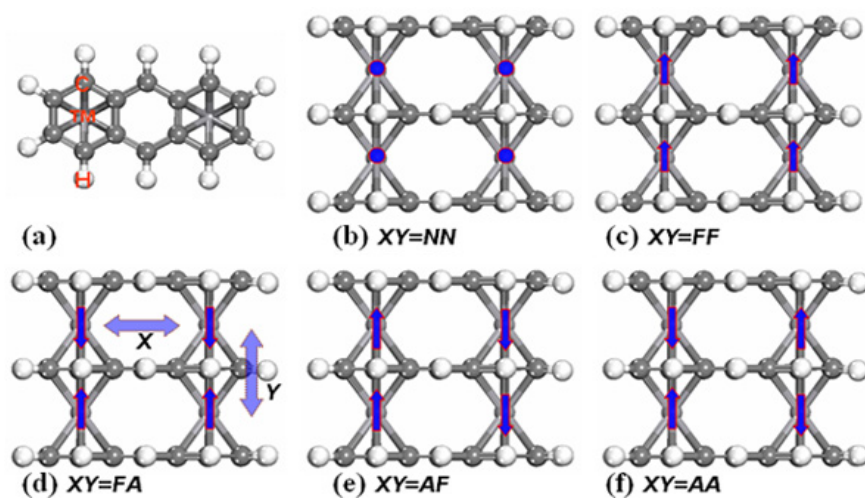


Fig. 2 Wang.eps

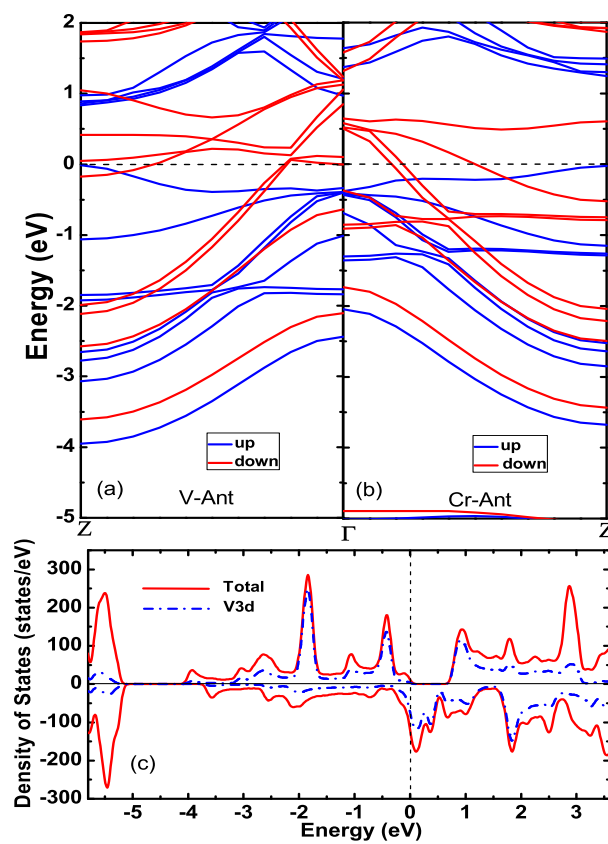


Fig. 3 Wang.eps

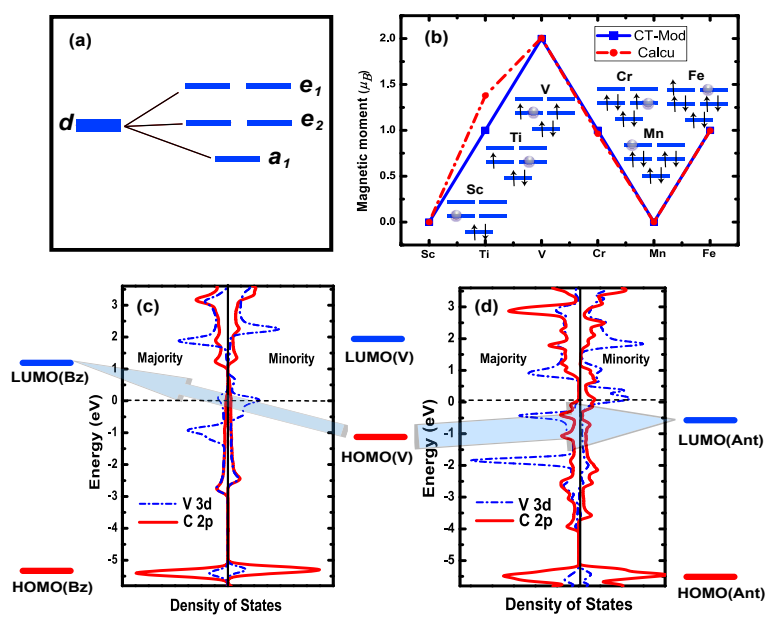


Fig. 4 Wang.eps

